

Toward extremes of angular momentum: Application of the Pfaffian algorithm in realistic calculations

Long-Jun Wang,¹ Fang-Qi Chen,^{1,2} Takahiro Mizusaki,³ Makito Oi,³ and Yang Sun^{1,4,*}

¹*Department of Physics and Astronomy, Shanghai Jiao Tong University, Shanghai 200240, People's Republic of China*

²*China Institute of Atomic Energy, Beijing 102413, People's Republic of China*

³*Institute of Natural Sciences, Senshu University, 3-8-1 Kanda-Jinbocho, Chiyoda-ku, Tokyo 101-8425, Japan*

⁴*Institute of Modern Physics, Chinese Academy of Sciences, Lanzhou 730000, People's Republic of China*

(Dated: July 14, 2014)

In a calculation of rotated matrix elements with angular momentum projection, the generalized Wick's theorem may encounter a practical problem of combinatorial complexity when the configurations have more than four quasi-particles (qps). The problem can be solved by employing the Pfaffian algorithm generally applicable to calculations of matrix elements for Hartree-Fock-Bogoliubov states with any number of qps. This breakthrough in many-body techniques enables studies of high-spin states in a shell-model framework. As the first application of the Pfaffian algorithm, the configuration space of the Projected Shell Model is expanded to include 6-qp states for both positive and negative parities. Taking ^{166}Hf as an example, we show that 6-qp states become the main configuration of the yrast band beyond spin $I \approx 34\hbar$, which explains the observed third back-bending in moment of inertia. Structures of multi-qp high- K isomers in ^{176}Hf are analyzed as another example.

PACS numbers: 21.10.Re, 21.60.Cs, 23.20.Lv, 27.70.+q

All nucleons of even-even nuclei couple pairwise in their ground state. Nuclear rotation brings an effect into the system that tends to break the nucleon pairs. This effect due to the rotation of nuclei was suggested in 1960 [1] in analogy to the electron pair breaking in superconductivity due to the existence of external magnetic fields. However, it was soon after realized that a sharp phase transition with pair collapse does not occur in nuclear systems due to the fact that nuclei have a finite size [2]. Another reason is that nucleons have an orbital angular momentum in addition to spin. The nucleons in the vicinity of the Fermi surfaces belong to subshells with rather different j -values, and therefore, they feel the Coriolis force very differently. Pairs in those orbitals with the highest angular momentum j , as for instance the neutron $i_{13/2}$ shell in the rare earth region, feel a strong Coriolis force, and therefore, break first (the Stephens-Simon effect [3]). They contribute to formation of 2-quasiparticle (qp) state as the main configuration of the yrast state. The Stephens-Simon effect [3] successfully explained the experimental observations of backbending in moment of inertia for rotating nuclei [4]. As a nucleus rotates faster and faster, subsequent pair-breakings can occur for the pairs from the next highest j orbitals. In the rare earth region, proton pairs in the $h_{11/2}$ shell are expected to break next, which was observed experimentally [5]. Measurements for further pair breakings at higher angular momenta are difficult. However, there have been early [6] and recent evidences [7, 8] of breaking of three nucleon pairs, which form 6-qp states as the main configuration of the yrast sequence.

Pair-breaking in nuclei can lead to formation of another special group of excited states: nuclear isomers. In a deformed potential a j -shell splits up into $2j+1$ K -states. Two or more states with high K quantum numbers can couple to form a high- K multi-qp configuration. The selection rules of elec-

tromagnetic decay hinder transitions from a high- K state to normal (low- K) states, resulting in a long-lived K isomer [9]. Understanding nuclear isomeric states is one of the current topics in nuclear structure and nuclear astrophysics, and also in potential applications [9–13]. The current experiments are able to find evidences for 6- or 8-qp isomers (see, for example, Refs. [14, 15]), and discoveries of more high- K isomers are expected from modern facilities such as the storage ring [16]. These data provide us with valuable information on the single-particle structure in deformed potentials.

On the theoretical side, it is a challenge to describe these phenomena in a shell-model framework if high-order qp states are involved. A theoretical problem lies in the procedure of computing the overlap matrix elements [17] between arbitrary multi-qp Hartree-Fock-Bogoliubov (HFB) states. The problem is known as follows. To study heavy, deformed nuclei, a practical way to build the model space is to start from a deformed single-particle basis (e.g. the solutions from a HFB or simply from the Nilsson+BCS method), and perform angular-momentum projection for the deformed qp states. Shell model diagonalization with a two-body Hamiltonian is then carried out in the projected multi-qp space. This is the basic concept of the Projected Shell Model (PSM) [18], which has been extensively applied to the structure study. However, since the involved overlap matrix elements of multi-qp states are usually calculated with the generalized Wick's theorem [18], one may encounter a practical problem of combinatorial complexity when more than 4-qp states are included in the basis configurations. For example, as many as hundreds (thousands) terms are to be considered to express each matrix element with 4-qp (6-qp) state. Therefore, up to recently, 3-qp (4-qp) states are selected among multi-qp configurations that can practically be treated in the PSM, for odd-mass (even-even) systems [19, 20].

To push the calculation further toward extremes of angular momentum involving higher order of qp states, a breakthrough in computational many-body techniques is needed. In

*Electronic address: sunyang@sjtu.edu.cn

nuclear structure physics, the Pfaffian concept has been introduced [21] as a key mathematical tool for solving the long-standing problem in the phase determination of the Onishi formula [22]. Moreover, it has been shown that the Pfaffian algorithm is very efficient also for calculating overlap matrix elements [23–28]. In particular, by means of Fermion coherent states and Grassmann integral, some of the present authors have derived an alternative approach to calculate the rotated matrix element for general qp states [29], which serves as a theoretical framework to extend the PSM model space.

Let us explain how the Pfaffian algorithm is applied to the PSM. The PSM employs the deformed Nilsson model [30] to generate a single-particle basis. Pairing correlations are incorporated into the Nilsson states by a BCS calculation. The Nilsson-BCS calculation defines a deformed qp basis from which the PSM model space is constructed. Three major harmonic-oscillator shells are taken in the calculation with $N = 4, 5, 6$ ($N = 3, 4, 5$) for neutrons (protons). Let us use $a_v^\dagger, a_\pi^\dagger$ (a_v, a_π) to denote neutron and proton qp creation (annihilation) operators associated with the qp vacuum $|\Phi\rangle$. The multi-qp configurations up to 6-qp states for even-even nuclei are given as follows:

$$\begin{aligned} & \{ |\Phi\rangle, a_{v_i}^\dagger a_{v_j}^\dagger |\Phi\rangle, a_{\pi_i}^\dagger a_{\pi_j}^\dagger |\Phi\rangle, a_{v_i}^\dagger a_{v_j}^\dagger a_{\pi_k}^\dagger a_{\pi_l}^\dagger |\Phi\rangle, \\ & a_{v_i}^\dagger a_{v_j}^\dagger a_{v_k}^\dagger a_{v_l}^\dagger |\Phi\rangle, a_{\pi_i}^\dagger a_{\pi_j}^\dagger a_{\pi_k}^\dagger a_{\pi_l}^\dagger |\Phi\rangle, \\ & a_{v_i}^\dagger a_{v_j}^\dagger a_{v_k}^\dagger a_{v_l}^\dagger a_{\pi_m}^\dagger a_{\pi_n}^\dagger |\Phi\rangle, a_{\pi_i}^\dagger a_{\pi_j}^\dagger a_{\pi_k}^\dagger a_{\pi_l}^\dagger a_{\pi_m}^\dagger a_{\pi_n}^\dagger |\Phi\rangle, \\ & a_{\pi_i}^\dagger a_{\pi_j}^\dagger a_{v_k}^\dagger a_{v_l}^\dagger a_{\pi_m}^\dagger a_{\pi_n}^\dagger |\Phi\rangle, a_{v_i}^\dagger a_{v_j}^\dagger a_{\pi_k}^\dagger a_{\pi_l}^\dagger a_{\pi_m}^\dagger a_{\pi_n}^\dagger |\Phi\rangle \}. \end{aligned} \quad (1)$$

where those 4-qp and 6-qp states from the fifth to tenth items in (1) are the new configurations introduced in the present work. Note that the PSM works with multiple harmonic-oscillator shells for both neutrons and protons. There are no restrictions in taking the indices v (for neutrons) and π (for protons) in (1); for example, a 2-qp state can be of positive parity if both quasiparticles i and j are from the major N -shells that differ in N by $\Delta N = 0, 2, \dots$, or of negative parity if i and j are from those N -shells that differ by $\Delta N = 1, 3, \dots$

The PSM wave function is a linear combination of projected states

$$|\Psi_{IM}^\sigma\rangle = \sum_{KK} f_{IK}^\sigma \hat{P}_{MK}^I |\Phi_K\rangle, \quad (2)$$

where $|\Phi_K\rangle$ are the multi-qp-states in (1). \hat{P}_{MK}^I is the angular momentum projection operator [17]

$$\hat{P}_{MK}^I = \frac{2I+1}{8\pi^2} \int d\Omega D_{MK}^I(\Omega) \hat{R}(\Omega), \quad (3)$$

with D_{MK}^I being the D -function [31], \hat{R} the rotation operator, and Ω the Euler angle. The energies and wave functions are obtained by solving the eigenvalue equation:

$$\sum_{K'K'} (H_{KK,K'K'}^I - E_I^\sigma N_{KK,K'K'}^I) f_{IK'}^\sigma = 0, \quad (4)$$

where $H_{KK,K'K'}^I$ and $N_{KK,K'K'}^I$ are respectively the projected matrix elements of the Hamiltonian and the norm

$$H_{KK,K'K'}^I = \langle \Phi_K | \hat{H} \hat{P}_{KK'}^I | \Phi_{K'} \rangle, \quad N_{KK,K'K'}^I = \langle \Phi_K | \hat{P}_{KK'}^I | \Phi_{K'} \rangle. \quad (5)$$

The central task in numerical calculations is to evaluate rotated matrix elements in the Hamiltonian and the norm

$$\mathcal{H}_{KK'} = \langle \Phi_K | \hat{H}[\Omega] | \Phi_{K'} \rangle, \quad \mathcal{N}_{KK'} = \langle \Phi_K | [\Omega] | \Phi_{K'} \rangle, \quad (6)$$

with the operator $[\Omega]$ defined as [18]

$$[\Omega] = \frac{\hat{R}(\Omega)}{\langle \Phi | \hat{R}(\Omega) | \Phi \rangle}. \quad (7)$$

$\mathcal{H}_{KK'}$ can be decomposed into terms of the “linked” contraction and $\mathcal{N}_{KK'}$ (see Appendix A.3 of Ref. [18] for details). An explicit example is for the evaluation of one-body operator \hat{O} , expressed as

$$\begin{aligned} \langle \Phi_K | \hat{O}[\Omega] | \Phi_{K'} \rangle &= \langle \Phi | \hat{O}[\Omega] | \Phi \rangle \langle \Phi_K | [\Omega] | \Phi_{K'} \rangle \\ &+ \sum_{ij} (\pm) (\hat{O}[\Omega] a_i^\dagger a_j^\dagger) \langle \Phi_K | [\Omega] | \Phi_{K'}(ij) \rangle \\ &+ \sum_{ij} (\pm) (a_i \hat{O}[\Omega] a_j^\dagger) \langle \Phi_K(i) | [\Omega] | \Phi_{K'}(j) \rangle \\ &+ \sum_{ij} (\pm) (a_i a_j \hat{O}[\Omega]) \langle \Phi_K(ij) | [\Omega] | \Phi_{K'} \rangle, \end{aligned} \quad (8)$$

where (\pm) is the parity of permutation. In Eq. (8), a state such as $|\Phi_{K'}(ij)\rangle$ means a one obtained by removing qps a_i^\dagger and a_j^\dagger from the state $|\Phi_{K'}\rangle$ to the “linked” contraction (expressed in round parentheses $(\hat{O}[\Omega] a_i^\dagger a_j^\dagger)$), which can be easily evaluated [18]). Thus, the main task concentrates on treating $\mathcal{N}_{KK'}$ efficiently. We can rewrite $\mathcal{N}_{KK'}$ as the following explicit form

$$\mathcal{N}_{KK'} = \langle \Phi | a_1 \cdots a_n [\Omega] a_{1'}^\dagger \cdots a_{n'}^\dagger | \Phi \rangle, \quad (9)$$

which is usually evaluated [18] by means of the generalized Wick’s theorem that decomposes Eq. (9) into a combination of three types of contraction, denoted as A , B , and C , with their matrix expressions [32]

$$\begin{aligned} A_{vv'}(\Omega) &\equiv \langle \Phi | [\Omega] a_v^\dagger a_{v'}^\dagger | \Phi \rangle = (V^*(\Omega) U^{-1}(\Omega))_{vv'}, \\ B_{vv'}(\Omega) &\equiv \langle \Phi | a_v a_{v'} [\Omega] | \Phi \rangle = (U^{-1}(\Omega) V(\Omega))_{vv'}, \\ C_{vv'}(\Omega) &\equiv \langle \Phi | a_v [\Omega] a_{v'}^\dagger | \Phi \rangle = (U^{-1}(\Omega))_{vv'}. \end{aligned} \quad (10)$$

where U and V are the corresponding matrices of action of the rotation operator on quasiparticles [32]. It was pointed out [29] that in applying the generalized Wick’s theorem, a matrix element of Eq. (9) involving n and n' qps, respectively in the left- and right-side of $[\Omega]$, contains $(n+n'-1)!!$ terms. The number of terms becomes so large that it is practically impossible to write down expressions explicitly for more than 4-qp states.

By using the Fermion coherent state and Grassmann integral, a general expression for the matrix elements (9) in terms of the Pfaffian can be derived [29]

$$\langle \Phi | a_1 \cdots a_n [\Omega] a_{1'}^\dagger \cdots a_{n'}^\dagger | \Phi \rangle = Pf(X) = Pf \begin{pmatrix} B & C \\ -C^T & A \end{pmatrix}, \quad (11)$$

where X is a skew-symmetric matrix with dimension $(n+n') \times (n+n')$. The indices of rows and columns for B run from 1 to n ($1, \dots, n$) and the ones for A run from $1'$ to n' ($1', \dots, n'$). For matrix C in Eq. (11), the indices of rows run from 1 to n and those of columns run from $1'$ to n' . The Pfaffian is defined as

$$Pf(\mathcal{A}) \equiv \frac{1}{2^n n!} \sum_{\sigma \in S_{2n}} \text{sgn}(\sigma) \prod_{i=1}^n a_{\sigma(2i-1)\sigma(2i)}. \quad (12)$$

for a skew-symmetric matrix \mathcal{A} with dimension $2n \times 2n$, of which matrix elements are a_{ij} . The symbol σ is a permutation of $\{1, 2, 3, \dots, 2n\}$, $\text{sgn}(\sigma)$ is its sign, and S_{2n} represents a symmetry group. This makes it possible and efficient to work with the expanded PSM configuration in (1), since calculations of the corresponding Pfaffian are not time-consuming [33]. Consequently, the new code still runs on a single core of PC although the configuration space in (1) is now much extended as compared to that of the original PSM code [34].

The PSM employs the Hamiltonian with separable forces:

$$\hat{H} = \hat{H}_0 - \frac{1}{2} \chi_{QQ} \sum_{\mu} \hat{Q}_{2\mu}^{\dagger} \hat{Q}_{2\mu} - G_M \hat{P}^{\dagger} \hat{P} - G_Q \sum_{\mu} \hat{P}_{2\mu}^{\dagger} \hat{P}_{2\mu}, \quad (13)$$

where \hat{H}_0 is the spherical single-particle term including the spin-orbit force [35], and the rest is the quadrupole+pairing type of separable interactions, which contains three parts. The strength of the quadrupole-quadrupole term χ_{QQ} is determined in a self-consistent manner so that it is related to deformation of the basis [18]. The monopole-pairing strength is taken to be the form $G_M = [G_1 \mp G_2(N-Z)/A]/A$, where “+” (“−”) is for protons (neutrons), with $G_1 = 20.12$ and $G_2 = 13.13$ being the coupling constants [36]. The quadrupole-pairing strength G_Q is taken, as usual, to be 16% of G_M for all the nuclei considered in this study.

If one keeps axial symmetry in the deformed basis, as it is the case of the present work, D_{MK}^I in Eq. (3) reduces to the small d -function and the three dimensions in Ω reduce to one. The following two examples represent first applications of the extension of the PSM configuration space with 6-qp's by using the Pfaffian algorithm.

In rotating nuclei, the Coriolis force tends to decouple the pairing. Nucleons in the highest- j orbital breaks first, leading to the first anomaly in observed moment of inertia at spin $I \approx 14$ in rare earth nuclei [4]. The phenomenon is usually displayed in an exaggerated manner with a back-bending plot, in which twice the moment of inertia 2Θ is plotted as a function of square of rotational frequency ω^2 . Figure 1 shows the back-bending plot for ^{166}Hf , where the theoretical results are compared with the experimental data. In the calculation, the deformation parameters $\varepsilon_2 = 0.208$ and $\varepsilon_4 = 0.013$ are taken from Ref. [37]. Anomalies in moment of inertia can be clearly seen as rotational frequency increases, roughly at $\omega^2 \approx 0.10$, 0.15 and 0.25, corresponding to spin $I \approx 12$, 24 and 34, respectively. The first anomaly exhibits the largest effect, causing a sharp increase in 2Θ within a small interval of ω^2 . This is known as the first back-bending, corresponding to breaking

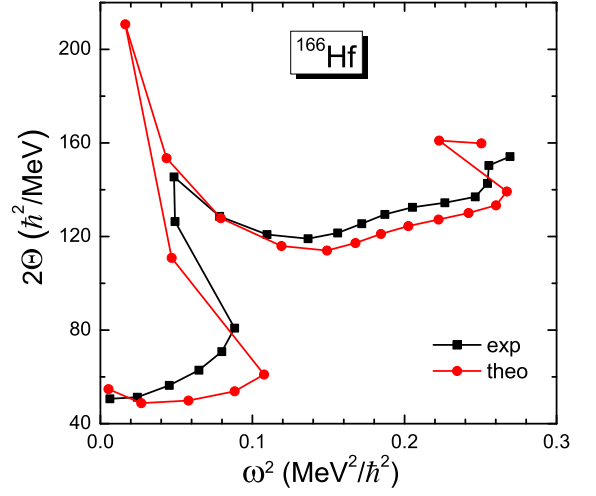


FIG. 1: (Color online) Back-bending plot for ^{166}Hf . The calculated results are compared with the experimental data taken from [7].

and alignment of a neutron $i_{13/2}$ pair. The experimental feature is described by the PSM calculation although quantitatively the theoretical results show deviations at low spins and exaggerate the back-bending. The discrepancy that the calculation shows a more flat curve at low spins could be attributed to the fact that the present calculation assumes an axially symmetric potential for deformed single-particle states, while triaxiality may have an effect on the low-lying states of this mass region [38]. The second anomaly in Fig. 1 corresponds to the small increase in 2Θ at $\omega^2 \approx 0.15$, which is nicely reproduced by the calculation. At this rotational frequency, an additional $h_{11/2}$ proton pair is broken and their spins are aligned along the axis of rotation. The third anomaly belongs to the few known cases that have ever been observed: 2Θ jumps suddenly again at $\omega^2 \approx 0.25$. The observation is correctly described by the present calculation, and is understood as a simultaneous breaking of two neutron $i_{13/2}$ pairs and one $h_{11/2}$ proton pair.

The calculated results can be analyzed by the so-called band diagram [18], where energies of theoretical bands are plotted as functions of spin. The energy of a theoretical band κ is defined as

$$E_{\kappa}(I) = \frac{\langle \Phi_{\kappa} | \hat{H} \hat{P}_{KK}^I | \Phi_{\kappa} \rangle}{\langle \Phi_{\kappa} | \hat{P}_{KK}^I | \Phi_{\kappa} \rangle}, \quad (14)$$

which is the projected energy of a multi-qp configuration in (1). Figure 2 displays the band diagram for ^{166}Hf , where the 0-qp ground (g-) band, one 2-qp band, one 4-qp band, and three 6-qp bands are selected from about 200 projected configurations in the calculation because of their important roles played in the yrast band (marked by dots). It is seen that the first back-bending at $I \approx 12$ in Fig. 1 corresponds to the crossing between g-band and the 2-qp (s-) band. The configuration of the s-band is found to be the neutron 2-qp state $\nu 3/2^+[651] \otimes \nu 5/2^+[642]$ with $K = 1$. The s-band remains to be the yrast band until it is crossed by a 4-qp band at $I \approx 24$. This 4-qp band is based on an addition

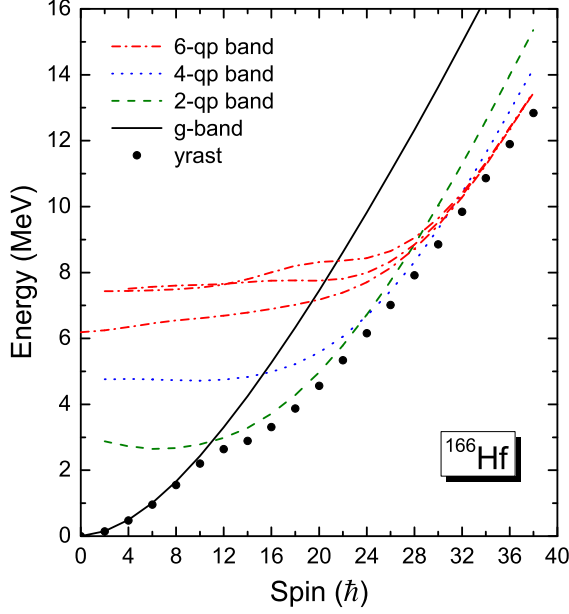


FIG. 2: (Color online) Band diagram for ^{166}Hf . Note that only even-spin states are plotted in order to avoid zigzag in these curves.

of an $h_{11/2}$ proton pair, corresponding to the configuration $\nu 3/2^+[651] \otimes \nu 5/2^+[642] \otimes \pi 7/2^-[523] \otimes \pi 9/2^-[514]$ with $K = 2$. Note that due to the small crossing angle (the ratio between the slopes of two crossing bands at the crossing point, see Ref. [39] for discussion), there is only a slight up-bending in 2Θ at $I \approx 24$, as seen in Fig. 1.

The contribution of the new 6-qp configurations in the basis enables us to understand the third anomaly in moment of inertia at $\omega^2 \approx 0.25$ in Fig. 1. It is clear that this anomaly corresponds to the crossing of the 4-qp band with three 6-qp bands at $I \approx 34$. Two of the 6-qp bands whose energies are almost the same at low spins have the same configuration $\nu 1/2^+[660] \otimes \nu 3/2^+[651] \otimes \nu 5/2^+[642] \otimes \nu 7/2^+[633] \otimes \pi 7/2^-[523] \otimes \pi 9/2^-[514]$ but with different K values $K = -1$ and -3 . The configuration of the third 6-qp band is $\nu 1/2^+[660] \otimes \nu 3/2^+[651] \otimes \nu 5/2^+[642] \otimes \nu 5/2^+[642] \otimes \pi 7/2^-[523] \otimes \pi 9/2^-[514]$ with $K = 0$. As the level density increases with spin, the wave function of the yrast band beyond $I \approx 34$ is found to have a large admixture of these 6-qp states. On the other hand, the 6-qp configuration consisting of $\nu(i_{13/2})^2 \nu(h_{9/2})^2 \pi(h_{11/2})^2$ lies higher in energy, and therefore, does not cross with the 4-qp band.

Our next example to demonstrate the role of 6-qp configurations is shown in Fig. 3 with the calculated multi-qp high- K bands in ^{176}Hf , compared with the experimental data taken from Ref. [40]. Several high- K 4-qp and 6-qp isomers in ^{176}Hf with higher excitation energies were experimentally known [41]. The quadrupole and hexadecapole deformation parameters for the ^{176}Hf calculation are adopted as $\epsilon_2 = 0.245$ and $\epsilon_4 = 0.024$, which are close to but slightly different from the deformation parameters in Ref. [37]. It is seen from Fig. 3 that the yrast band is well reproduced by the PSM calculation. In consistence with Ref. [40], our calculation suggests that

the 2-qp $K^\pi = 6^+$ and 8^- states have $\pi 7/2[404] \otimes \pi 5/2[402]$ and $\pi 7/2[404] \otimes \pi 9/2[514]$, respectively, as the main configurations for the observed bands.

For the $K^\pi = 15^+$ band, the proposed configuration in Ref. [40] was a 4-qp $\nu 5/2^-[512] \otimes \nu 9/2^+[624] \otimes \pi 7/2^+[404] \otimes \pi 9/2^-[514]$. Our calculated band-head energy for this configuration (indicated by cal) is about 700 keV higher than the corresponding data. The calculation shows that there is another 4-qp configuration (indicated by cal[#]) with $\nu 7/2^-[514] \otimes \nu 7/2^+[633] \otimes \pi 7/2^+[404] \otimes \pi 9/2^-[514]$, which is the lowest one among the same type of configuration (i.e. of the four constituent quasi-particles originating from the orbitals belonging to four different major shells). As the band associated with this configuration lies lower in energy, it should have a larger chance to be observed in experiment.

The rotational band built on the $K^\pi = 14^-$, 2866-keV isomer was observed up to $I = 20$ [41]. One can see from Fig. 3 that both the excitation energy of this isomer and the corresponding rotational band are well reproduced by the calculation. The configuration is found to be the 4-qp $\nu 5/2^-[512] \otimes \nu 7/2^-[514] \otimes \pi 7/2^+[404] \otimes \pi 9/2^-[514]$, consistent with the one suggested in Ref. [40]. Nevertheless, the calculated moment of inertia is smaller than the corresponding experimental value, i.e., the calculated level spacings between adjacent levels of the band is larger than the experimental ones. The same problem seems to exist in the above-discussed $K^\pi = 15^+$ 4-qp band. Such a discrepancy could be due to the fact that pairing correlations are treated by the BCS method in the present model, which does not account for the blocking effects properly.

At least three 6-qp structures have been known in ^{176}Hf [40]: the 4377-keV $K^\pi = 19^+$ and 4864-keV $K^\pi = 22^-$ isomers, and the 4767-keV $K^\pi = 20^-$ state. In Fig. 3, we show the predicted rotational bands based on these configurations. The calculation suggests that the band built on the $K^\pi = 19^+$ isomer has the main configuration $\nu 1/2[521] \otimes \nu 5/2[512] \otimes \nu 7/2[514] \otimes \nu 9/2[624] \otimes \pi 7/2[404] \otimes \pi 9/2[514]$, consistent with the assignment given in Ref. [40]. The 6-qp isomer with $K^\pi = 22^-$ was assigned to be of the configuration $\nu 5/2^-[512] \otimes \nu 7/2^-[514] \otimes \nu 7/2^+[633] \otimes \nu 9/2^+[624] \otimes \pi 7/2^+[404] \otimes \pi 9/2^-[514]$. The experimental energy of this isomer is well reproduced by the PSM. This isomer is found to decay to the $K^\pi = 20^-$ state by $E2$ transition [40]. The configuration of the $K^\pi = 20^-$ state was assigned to be $\nu 1/2^-[521] \otimes \nu 7/2^-[514] \otimes \nu 7/2^+[633] \otimes \nu 9/2^+[624] \otimes \pi 7/2^+[404] \otimes \pi 9/2^-[514]$ [40]. The calculated excitation energy for this configuration is found to be slightly higher than another 6-qp configuration $\nu 5/2^-[512] \otimes \nu 7/2^-[514] \otimes \nu 5/2^+[642] \otimes \nu 7/2^+[633] \otimes \pi 7/2^+[404] \otimes \pi 9/2^-[514]$ (indicated by cal[#]).

Calculated $E2$ transition probabilities associated with isomer decay are compared with available experimental data in Table I. The first three transitions in Table I are K -forbidden ones with $\Delta K = 6$. Our calculated results are 1-3 orders of magnitude smaller than the data. Again, we attribute such a discrepancy to the absence of triaxial degree of freedom in the deformed basis. In Ref. [38], it was demonstrated that the K -forbidden transition from the 6^+ 2-qp isomer to the

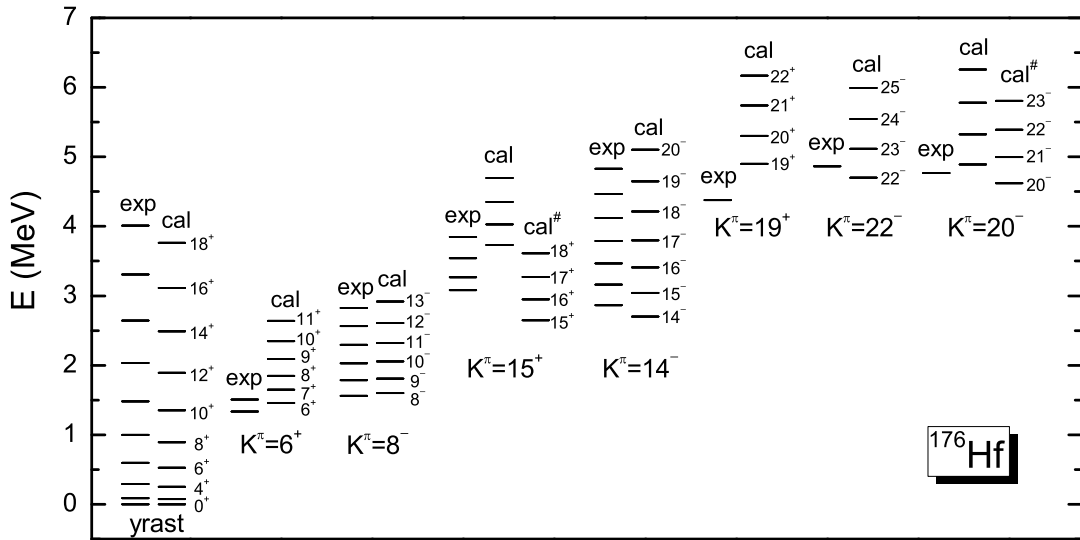


FIG. 3: Comparison of the calculated yrast, 2-q, 4-q, and 6-q bands for ^{176}Hf with available experimental data taken from [40].

TABLE I: Comparison of calculated $B(E2)$ values (in W.u.) for the isomeric states in ^{176}Hf with the available data taken from [40, 42].

K_i^π	I_i	K_f^π	I_f	$B(E2; I_i \rightarrow I_f)$	
				exp.	cal.
6^+	6	0^+	6	2.82×10^{-6}	1.93×10^{-9}
6^+	6	0^+	4	3.16×10^{-7}	2.21×10^{-9}
14^-	14	8^-	12	5.33×10^{-7}	5.55×10^{-8}
22^-	22	20^-	20	4.8×10^{-3}	3.7×10^{-2}

ground-state band is sensitive to mixing with the 6^+ state of the γ -vibrational band, which could be accounted for when a triaxial deformed single-particle basis with three-dimensional angular momentum projection is employed in the model. On the other hand, the calculated $B(E2)$ for the allowed transition from the 22^- isomer to the 20^- state is 3.7×10^{-2} W.u., in a reasonable agreement with the experimental value 4.8×10^{-3} W.u. obtained in [40].

In summary, the Pfaffian algorithm has been recently introduced to facilitate computer codings in realistic shell-model calculations. By using the Pfaffian algorithm for computing

overlap matrix elements, the configuration space of the PSM has been expanded, for the first time, to include all kinds of 4-q and some 6-q states for both positive and negative parities. As an initial application, contributions of the 4-q and 6-q states in the yrast band at high spins have been analyzed. It is found that the third anomaly in moment of inertia at spin $I \approx 34$ in ^{166}Hf could be explained as the band crossing with the 6-q bands. Multi-q high- K isomers in ^{176}Hf have also been investigated, where the experimentally observed high- K isomers at high excitation energies have been described as various 2-, 4-, and 6-q configurations.

The present work has been restricted in the axial symmetric case in the deformed basis. The current studies of the Triaxial PSM can only afford to use a very small multi-q configuration space [38, 43]. It remains to be seen how the Pfaffian algorithm can help to simplify the calculation with angular momentum projection in a three-dimensional space.

Valuable discussions with Z.-C. Gao and Q.-L. Hu are acknowledged. Research at SJTU was supported by the National Natural Science Foundation of China (No. 11135005) and by the 973 Program of China (No. 2013CB834401).

-
- [1] B. R. Mottelson and J. G. Valatin, Phys. Rev. Lett. **5**, 511 (1960).
 - [2] U. Mutz and P. Ring, J. Phys. G: Nucl. Phys. **10**, L39 (1984).
 - [3] F. S. Stephens and R. S. Simon, Nucl. Phys. A **183**, 257 (1972).
 - [4] A. Johnson, H. Ryde, and J. Sztarkier, Phys. Lett. **34B**, 605 (1971); A. Johnson, H. Ryde, and S. A. Hjorth, Nucl. Phys. A **179**, 753 (1972).
 - [5] I. Y. Lee *et al.*, Phys. Rev. Lett. **38**, 1454 (1977).
 - [6] J. Burde *et al.*, Phys. Rev. Lett. **48**, 530 (1982).
 - [7] D. R. Jensen *et al.*, Eur. Phys. J. A **8**, 165 (2000).
 - [8] R. B. Yadav *et al.*, Phys. Rev. C **80**, 064306 (2009).
 - [9] P. M. Walker and G. D. Dracoulis, Nature **399**, 35 (1999).
 - [10] A. Aprahamian and Y. Sun, Nat. Phys. **1**, 81 (2005).
 - [11] P. M. Walker and J. J. Carroll, Phys. Today **58** (2005).
 - [12] F. R. Xu, E. G. Zhao, R. Wyss, and P. M. Walker, Phys. Rev. Lett. **92**, 252501 (2004).
 - [13] R. D. Herzberg *et al.*, Nature **442**, 896 (2006).
 - [14] C. S. Purry *et al.*, Phys. Rev. Lett. **75**, 406 (1995).
 - [15] G. D. Dracoulis *et al.*, Phys. Rev. C **71**, 044326 (2005).
 - [16] M. W. Reed *et al.*, Phys. Rev. Lett. **105**, 172501 (2010).
 - [17] P. Ring and P. Schuck, *The nuclear many-body problem* (Springer Verlag, 2004).

- [18] K. Hara and Y. Sun, *Int. J. Mod. Phys. E* **4**, 637 (1995).
- [19] F.-Q. Chen, Y.-X. Liu, Y. Sun, P. M. Walker, and G. D. Dracoulis, *Phys. Rev. C* **85**, 024324 (2012).
- [20] Y.-X. Liu, Y. Sun, X.-H. Zhou, Y.-H. Zhang, S.-Y. Yu, Y.-C. Yang, H. Jin, *Nucl. Phys. A* **858**, 11 (2011).
- [21] L. M. Robledo, *Phys. Rev. C* **79**, 021302(R) (2009).
- [22] N. Onishi and S. Yoshida, *Nucl. Phys.* **80**, 367 (1966).
- [23] L. M. Robledo, *Phys. Rev. C* **84**, 014307 (2011).
- [24] G. F. Bertsch and L. M. Robledo, *Phys. Rev. Lett.* **108**, 042505 (2012).
- [25] B. Avez and M. Bender, *Phys. Rev. C* **85**, 034325 (2012).
- [26] M. Oi and T. Mizusaki, *Phys. Lett. B* **707**, 305 (2012).
- [27] T. Mizusaki and M. Oi, *Phys. Lett. B* **715**, 219 (2012).
- [28] Q.-L. Hu, Z.-C. Gao, and Y. S. Chen, *Phys. Lett. B* **734**, 162 (2014).
- [29] T. Mizusaki, M. Oi, F. Q. Chen, and Y. Sun, *Phys. Lett. B* **725**, 175 (2013).
- [30] S. G. Nilsson *et al.*, *Nucl. Phys. A* **131**, 1 (1969).
- [31] D. A. Varshalovich, A. N. Moskalev, and V. K. Khersonskii, *Quantum theory of angular momentum* (World Scientific, 1988).
- [32] K. Hara and S. Iwasaki, *Nucl. Phys. A* **332**, 61 (1979).
- [33] C. González-Ballester, L. M. Robledo, and G. F. Bertsch, *Comput. Phys. Commun.* **182**, 2213 (2011).
- [34] Y. Sun and K. Hara, *Comput. Phys. Commun.* **104**, 245 (1997).
- [35] T. Bengtsson and I. Ragnarsson, *Nucl. Phys. A* **436**, 14 (1985).
- [36] Y. Sun and D. H. Feng, *Phys. Rep.* **264**, 375 (1996).
- [37] P. Moller, J. R. Nix, W. D. Myers, and W. J. Swiatecki, *At. Data Nucl. Data Tables* **59**, 185 (1995).
- [38] F.-Q. Chen, Y. Sun, P. M. Walker, G. D. Dracoulis, Y. R. Shimizu, and J. A. Sheikh, *J. Phys. G: Nucl. Part. Phys.* **40**, 015101 (2013).
- [39] K. Hara and Y. Sun, *Nucl. Phys. A* **529**, 445 (1991).
- [40] G. Mukherjee *et al.*, *Phys. Rev. C* **82**, 054316 (2010).
- [41] T. L. Khoo, F. M. Bernthal, R. G. H. Robertson, and R. A. Warner, *Phys. Rev. Lett.* **37**, 823 (1976).
- [42] M. S. Basunia, *Nucl. Data Sheets* **107**, 791 (2006).
- [43] J. A. Sheikh, G. H. Bhat, Y.-X. Liu, F.-Q. Chen, Y. Sun, *Phys. Rev. C* **84**, 054314 (2011); J. A. Sheikh, G. H. Bhat, Y. Sun, R. Palit, *Phys. Lett. B* **688**, 305 (2010).